UNCLASSIFIED

~~70-01570~~

CR-103091

APPENDIX D AND APPENDIX E
ADDENDA
TO
FINAL REPORT

DEVELOPMENT OF CO_2 LASER DOPPLER INSTRUMENTATION DETECTION OF CLEAR AIR TURBULENCE

ER70-4203 5 June 1970

RAYTHEON

RAYTHEON COMPANY
EQUIPMENT DIVISION

RAYTHEON COMPANY
EQUIPMENT DIVISION

APPENDIX D AND APPENDIX E
ADDENDA
TO
FINAL REPORT

DEVELOPMENT OF CO_2 LASER DOPPLER INSTRUMENTATION DETECTION OF CLEAR AIR TURBULENCE

ER70-4203

5 June 1970

CONTRACT NAS-8-24742

Prepared for

GEORGE C. MARSHALL SPACE FLIGHT CENTER
NASA
Huntsville, Alabama 35812

Prepared by

Dr. C. Sonnenschein
A. Jelalian
Dr. W. Keene

RAYTHEON COMPANY
EQUIPMENT DIVISION
EQUIPMENT DEVELOPMENT LABORATORY
Sudbury, Massachusetts 01776

APPENDIX D

PRELIMINARY PROGRAM DEVELOPMENT PLAN

D.1 INTRODUCTION

Over the past several years, much activity has been directed toward the utilization of electro-optical techniques for the measurement of clear-air turbulence. By using a laser-doppler heterodyne approach, a research type instrument capable of being flown on a 707-type aircraft can be developed.

Particularly pertinent to this program development plan are the following:

1. Demonstrated measurements of doppler returns from clear air.
2. Demonstrated remote measurement of trailing vortices.
3. Technology developments in the field of CO_2 laser technology.

D.2 WORK SCHEDULES AND TASKS

The subsequent program consisting of schedules and tasks makes use of prior efforts as well as advanced electro-optic techniques for performing measurements of clear-air turbulence.

D.2.1 SCHEDULES

A program plan to develop an experimental "flyable" pulse doppler laser research system capable of measuring clear-air turbulence can be time-phased to allow this development to occur within 14 months after contract award. A detailed schedule of this program phase is shown in Figure D-1. In order to provide a comprehensive program overview a GANT chart is provided in Figure D-2 which illustrates a schedule resulting in an operational,

RAYTHEON COMPANY — PLANNING SCHEDULE — CLASSIFICATION: DATE:

REFERENCE | UNIT / TASK LASER DOPPLER CAT PROGRAM

PERIOD ENDING

REVIEW DATES: 1 2 3 4 5 6 7 8 9 10 11 12 13 14 15 16 17 18 19 20 21

MAJOR MILESTONES

- MASTER OSCILLATOR COMPLETED
- POWER AMPLIFIER COMPLETED
- MOPA CHAIN INTEGRATED
- RECEIVER DESIGNS COMPLETED
- FLIGHT TEST RACKS COMPLETED
- GROUND TESTS COMPLETED
- AIRCRAFT INSTALLATION TESTS STARTED

I. MOPA CHAIN
- 1. MASTER OSCILLATOR
  - a. OPTO-MECHANICAL DESIGN
  - b. LONG LEAD ITEM PROCUREMENT
  - c. FABRICATION
  - d. ASSY., ALIGN., + TEST
- 2. POWER AMPLIFIER
  - a. OPTO-MECHANICAL DESIGN
  - b. LONG LEAD ITEM PROCUREMENT
  - c. FABRICATION
  - d. ASSY., ALIGN., + TEST
- 3. POWER SUPPLY
  - a. ELECTRONICS DESIGN
  - b. MECHANICAL DESIGN
  - c. ~~BALLAST DESIGN~~
  - d. SWITCHING CONTROLS
  - e. PURCHASE
  - f. TEST
- 4. E/O MODULATOR
  - a. PURCHASE PARTS
  - b. FABRICATION
  - c. TIMING + SYNC. DESIGN
  - d. TEST
- 5. MOPA CHAIN INTEGRATION

II. OPTICS DESIGN + DEVELOPMENT
- 1. OPTICS + TELESCOPES
- 2. DETECTOR + DEWAR

FOLDOUT FRAME

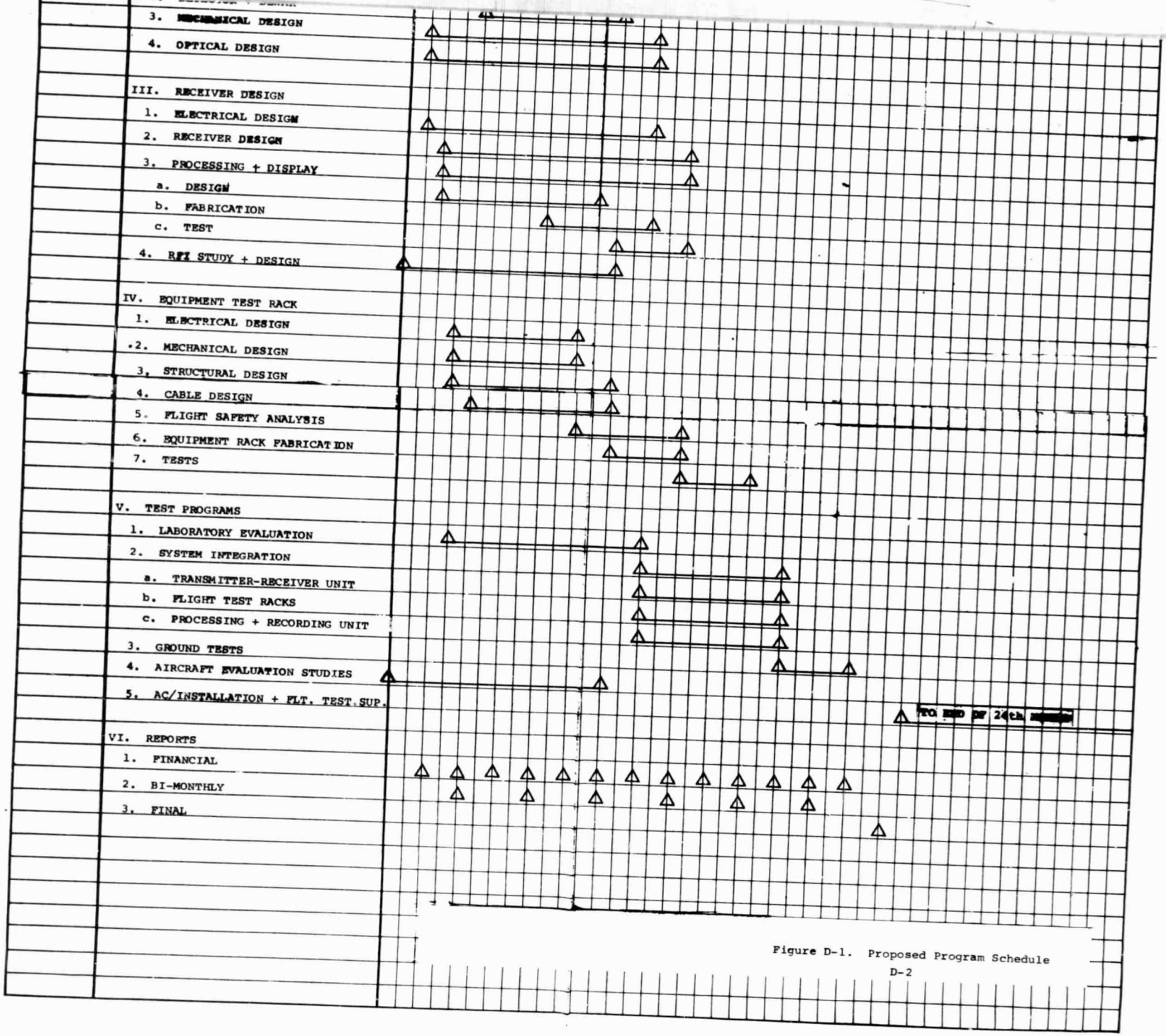

Figure D-1. Proposed Program Schedule

REFERENCE	UNIT / TASK LASER DOPPLER CAT PR
	PERIOD E
	REVIEW D
	I. RESEARCH SYSTEM
	1. TRANSMITTER DEVELOPMENT
	a. DESIGN + FAB. TRANSMITT
	b. DESIGN + FAB. POWER SUP
	+ TIMING CONTROLS
	c. MOPA CHAIN INTEGRATION
	2. OPTICS DESIGN + DEVELOPME
	3. RECEIVER DESIGN
	4. FLIGHT TEST EQUIP. DESIGN
	5. LABORATORY EVALUATIONS
	6. SYSTEM INTEGRATION
	7. GROUND TEST
	8. A/C FLIGHT TESTS
	II. PROTOTYPE DEVELOPMENT PROG
	LONG LEAD ITEM PROCURE.
	SYSTEM ANALYSIS
	FINALIZE SPECS
	GEN. EQUIP. DEV. (BREADBOA
	ELEC. + MECH. DESIGN EVAL.
	MAX-MIN TOLERANCE DESIGN
	FAB. THERMAL/STRUCT. MODEL
	TEST THERMAL/STRUCT. MODEL
	PRELIMINARY DESIGN REVIEW
	ENG. MODEL DEV. RELEASE
	ENG. MODEL FAB. + ASSY.
	SYS. INTEGRATION ENG. MODE
	SYS. VERIFICATION (C.D.R.)
	PROCURE PROTO. MDL. PARTS
	FAB. + ASSY. PROTO. MODEL
	PROTO. SYSTEM INTEGRATION
	ACCEPT. TEST PROTO.
	QUAL. TEST PROTO. (FAC)
	FAB. + ASSY. DELIVERABLE
	SYSTEM INTEG. DELIVERABLE
	ACCEPTANCE TEST DELIVERABL
	FINAL REPORT
	TEST EQUIP.
	MAJOR MILESTONES
	INTEGRATED FOLDED MOPA CHA
	EXPERIMENTAL SYST. FLT. TE
	PROTOTYPE DEV. PROG. START
	PRELIMINARY DESIGN RELEASE
	CRITICAL DESIGN RELEASE
	FIRST ARTICLE CONFIGURATIO

FOLDOUT FRAME

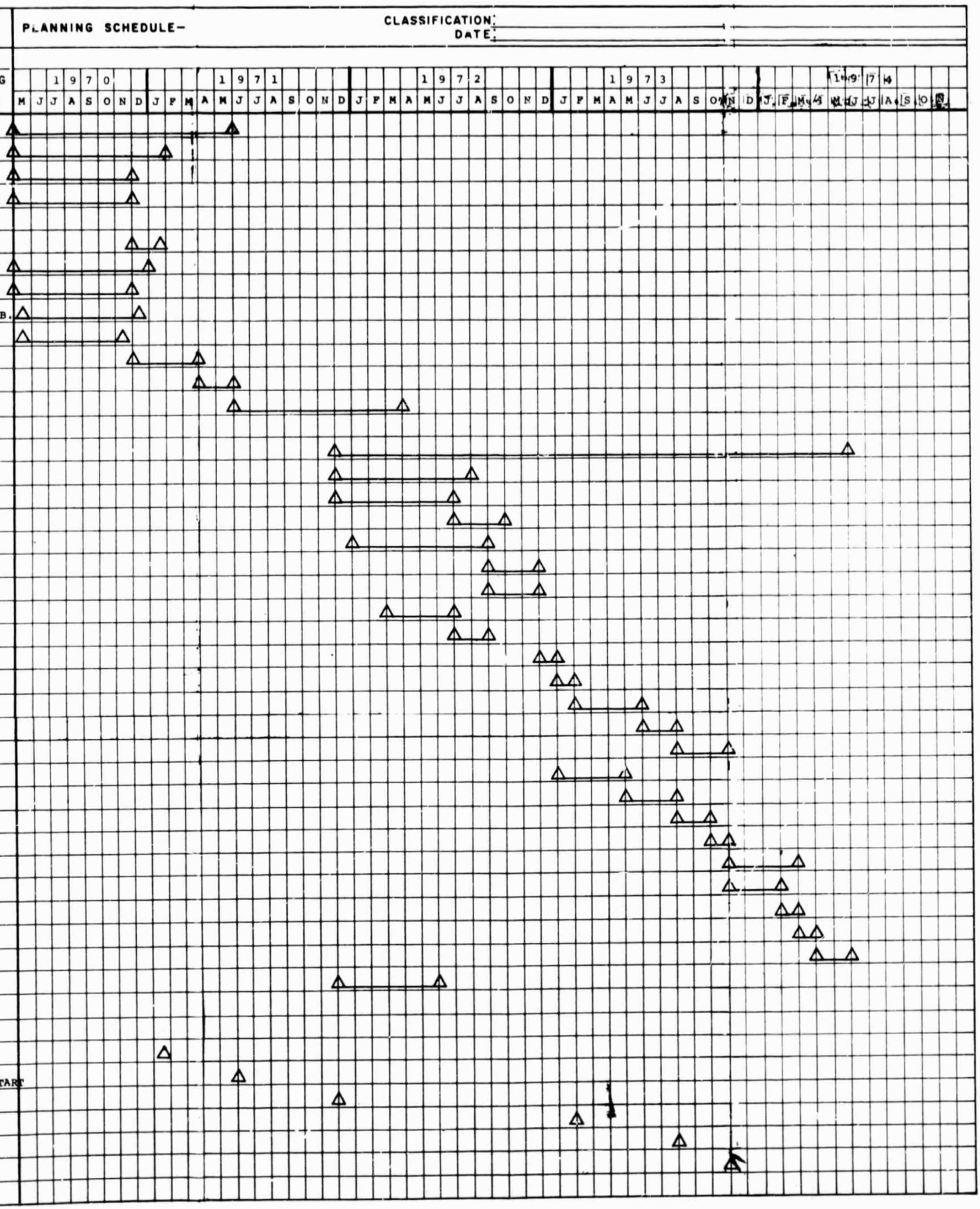

Figure D-2. Operational CAT System Program Schedule

FOLDOUT FRAME -2

qualified CAT system in 4.1 years. This unit would be qualified environmentally to the appropriate military and/or FAA specifications. The first phase illustrated in Figure D-1 is devoted to the demonstration of this system capability of detecting clear-air turbulence.

D.2.2 TASKS

This section discusses the work tasks involved in order to design, fabricate, test and deliver one experimental engineering model of the CAT pulse doppler laser radar. The detection instrument utilizing the system design studies and the information obtained from the transmitter feasibility demonstration tests performed under NASA Contract NAS8-24742 are best described in terms of two major subsystems: the transmitter and receiver. Commencing with the transmitter, the following proposed work tasks are recommended:

D.2.2.1 Transmitter

Basically the frequency stability and overall design of the transmitter should be compatible with an on-board aircraft system (707 type) and consist of (1) a CO_2 laser master oscillator, (2) a modulator, (3) a folded laser amplifier, (4) heterodyne recombination optics, and (5) external optics -- including a telescope and manual scanner. Each unit of the transmitter is briefly described.

D.2.2.1.1 Master Oscillator

A master oscillator, having single-mode, single-frequency, CO_2 CW laser and a rigid frequency stability, should be fabricated. The oscillator, moreover, should be compatible with an on-board aircraft system (707 type). Ideally, the unit should have an output power of approximately 10 watts.

D.2.2.1.2 Electro-Optical Modulator

The modulator evaluation conducted under phase one of the CAT program resulted in the choice and purchase of an E/O modulator and the circuit design of the modulator driver. Under this phase of the program the modulator electronics should be fabricated and tested, to allow 1 - 10 μsec output driver pulses; additionally, selected pulse width controls of 2-μs, 4-μs and 8-μs time duration should be designed into this unit to allow in-flight pulse width selection.

D.2.2.1.3 Folded Laser Power Amplifier

A power amplifier modeled from the test data obtained from the feasibility demonstration should be designed to be compatible with the overall system and consist of eight folded 3.5-foot sections of discharge tubes. This unit should be integrated with the master oscillator and electro-optical modulator in an acoustically and RFI shielded enclosure. This folded power amplifier should also be capable of providing 10-mj pulses with variable pulse width.

D.2.2.1.4 Heterodyne Recombination Optics

A circular polarization is recommneded for flight instrumentation. By means of several multi-directional translation stages and double-angle adjustments for component positioning, flexibility of component installation and alignment should be provided in the output end of the transmitter. Since the CAT detection system is a very long interferometer, it must be maintained in diffraction-limited alignment in order to accomplish doppler heterodyne detection.

D.2.2.1.5 Optics and Telescope

The optical design can be logically separated into two portions: optics internal to the lasers, and external optics. The

internal optics have been specified during the first phase of this program, and their purchase and further opto-mechanical design should be performed under the power amplifier and master oscillator tasks. The optics and telescope task should include the design, purchase, and assembly of all external optical elements.

D.2.2.2 Electro-Optical Receiver

The electro-optical portion of the receiver contains the optical detector, a low-noise wide-band preamplifier, and a local oscillator and mixer to heterodyne the detector signal to the IF band, signal processors, signal display, and recording apparatus. After a detector has been selected, so that its gain and responsivity are known, the detector biasing and matching networks should be designed and built. Noise measurements will then enable the selection and purchase of an appropriate preamplifier, mixer, and i-f oscillator.

Basically, the receiver operates by determining the bandwidth of the received doppler-shifted signal beam and from this information generates range-velocity data appropriate for (1) real time display on a CRT in the aircraft, and (2) recording purposes for post-flight analysis. In a flight test program the aircraft should also be instrumented with vibration measurement apparatus whose recorded output would be correlated with the CAT research instrument recorded output, and with the appropriate time phase corresponding to the range to the target.

D.2.2.3 Transmitter and Receiver Integration

The transmitter and receiver should be integrated in order to realize a CAT research instrument. Laboratory feasibility tests should be performed where necessary directed toward development of the system. Additionally, ground tests, check-out, and calibration tasks will be carried out.

It is assumed that the particular 707-type aircraft to be used for the flight test program will be selected by NASA and made available for inspection early in the program. Both the design and packaging configuration of the instrument and the successful execution of the airplane-laser CAT system compatibility studies depend strongly on the test aircraft selected. A block diagram of the recommended system appears in Figure D-3. Basically the unit is composed of a transmitter-receiver unit and four flight test equipment consoles.

The experimental flight test system consists of a pulsed CO_2 laser transmitter, an electronically gated heterodyne receiver and appropriate electronics to perform the necessary signal processing. The transmitter frequency stability is derived from a CW CO_2 sealed master oscillator. The CW polarized output of this laser will be modulated by the electro-optical gallium arsenide modulator to provide variable pulse width. The pulsed energy output of the 5-mm modulator will then be beam expanded to 15 mm to allow optimum coupling into the power amplifier. To help provide isolation, the linearly polarized output of the power amplifier will be changed to circular polarization before it is transmitted through a 12-inch telescope and into the atmosphere.

The return scattered signal is collected through the same optical system, combined with a portion of the master oscillator and directed to an optical detector. The electrical output of this detector is amplified and heterodyned (this time with a microwave local oscillator) to an I.F.

The IF signal will then be amplified and analyzed by a filter bank appropriately matched to the pulse length. The output of each filter is individually detected and appropriately displayed. This display may take the form of an RVI, where velocity is plotted as a function of range; an A-scope, where amplitude vs velocity is displayed in a single range cell, and/or a digital

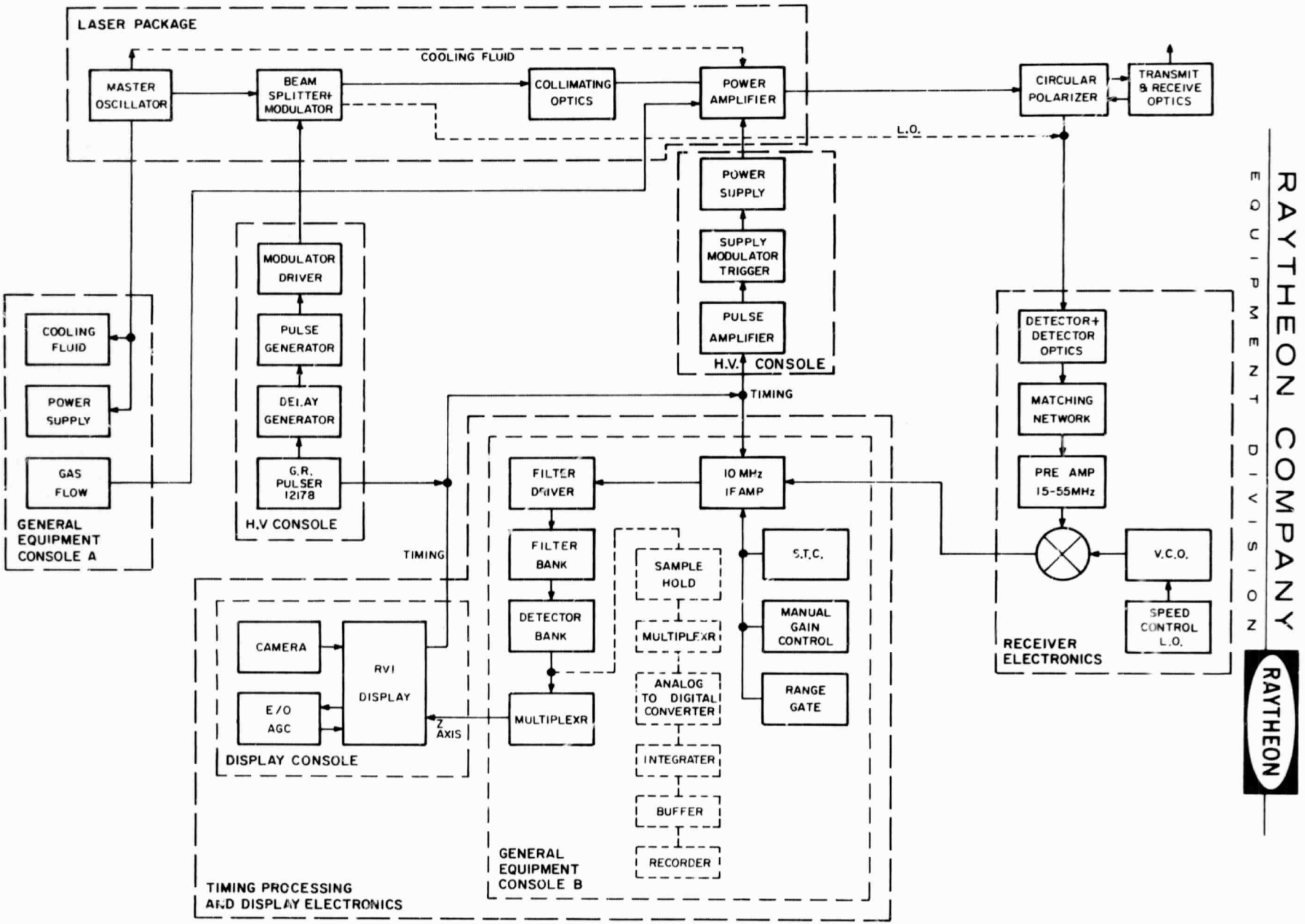

Figure D-3. System Block Diagram

tape recorder, which will contain the velocity information in a single range cell.

D.2.2.4 Flight Test Equipment Racks

Four equipment consoles would be required to house the necessary supporting equipment to power, control, monitor, process and display the data obtained from the transmitter-receiver unit. The transmitter-receiver unit is composed of the master-oscillator, power amplifier, E/O modulator, optics detector and dewar and receiving electronics. This effort would represent the work involved in the mechanical, structural, thermal and electrical designs of the equipment consoles, which are composed of several H.V. and L.V. power supplies, a spectrum analyzer, oscilloscope, a modulator driver unit, meter and control panel, vacuum pump, flow gauges and pressure valves, and the electronic processing equipment.

The electrical design effort should involve the electrical design, fabrication and test of the equipment consoles, including cabling, grounding and shielding requirements and console interconnections.

The structural design effort consists of defining the structural design criteria, performing a mass property analysis, a dynamic load analysis, a static stress analysis, and preparing a flight safety analysis.

The thermal design activity consists of providing thermal design services to the product design functions, determining fan-motor selection, ducting, and similar effort for the transmitter-receiver units and four flight test equipment consoles.

The mechanical design effort consists of specifying and performing the test equipment console layouts, sizing and purchasing the RFI cabinets, designing a shock mount technique consistent with the structural design task, provide pump mounts and pressure bottle restraints.

All equipment to be mounted in these racks should be of standard 19-inch front panel design. Equipment purchased in this standard panel size will not be redesigned. Additionally, because equipment reproducibility is not considered a requirement, good engineering sketches will be utilized as opposed to formal drawings.

D.2.2.5 Electronics Receiver Processing

In the first phase of this contract, a receiver for the CAT system was analyzed and designed to achieve a sufficient detection probability with a low false-alarm rate. The receiver consisted of a set of filters, appropriate amplifiers, and an RVI display. The receiver design should be implemented in this phase of the program. Also, the various components should be purchased, assembled, and tested to assure satisfactory performance.

The receiver to be built should be a versatile device, capable of processing the scattered returns from pulses of various lengths. This capability will ensure operation despite uncertainties in the properties of the atmosphere.

The display recommended for use with the receiver is a range-velocity type which portrays velocity distribution at all ranges within the limits of system operation. Additionally, this same approach is compatible with a selected single range gate technique which would allow a signal amplitude-velocity A scope presentation. Recording of the RVI display should be performed photographically with a scope camera. Also, an option should be available to allow a digital tape recording of the velocity distribution in a single range cell. The tape from this channel will allow a permanent record in digital form that can be processed after the flight test for additional information.

D.2.2.6 System Analysis Effort

This effort should provide analytical support to the program in the following areas:

1. Perform the necessary airplane interface analysis.

2. Continue to update receiver analysis work with additional meteorological information as it is obtained from both the Marshall Space Flight Center and other sources.

3. Perform troubleshooting analysis support to the laboratory feasibility tests and system integration tests.

4. Establish test procedures and evaluate test data for the ground tests.

D.2.2.7 Test Programs

Lab Feasibility - During the program a series of laboratory feasibility experiments should be carried out to test the various components. The data from these tests will be evaluated to ensure the proper functioning of the individual components as well as their proper performance in the system.

System Integration - The tests performed should concern the functioning of the components in the framework of the total system. These results should be analyzed from the point of view of optimizing the overall system performance.

Ground Test - The assembled system should be tested on the ground to predict its behavior in an aircraft environment. Test results should be analyzed to determine the ability of the system to detect clear-air turbulence.

APPENDIX E

EFFECT OF MECHANICAL VIBRATIONS ON A LASER TRANSMITTER FOR CAT

E.1 INTRODUCTION

Vibrations within an optical transmitter, such as the laser oscillator-amplifier chain of the CAT laser radar system, react more critically upon certain components than others. Most seriously affected is the laser master oscillator, due to its resonant nature which depends critically upon mechanical tolerances. Such resonances are characterized by extremely high Q's, quantities which are inversely proportional to the fractional change in cavity length required to shift the laser output frequency by one line width. By comparison, laser amplifier units within the chain possess much lower Q's. They possess no end mirrors to produce a cavity resonance, and are therefore characterized by the much broader atomic resonance. In a rough sense, the length change necessary to produce a noticeable alteration in amplifier characteristics and the length change needed to perturb the oscillator, both vary inversely with their respective Q's. Accordingly, the amplifier's susceptibility to mechanical vibrations is not nearly so critical as in the case of the master oscillator. Pulse-forming switches meanwhile are even less critically affected by vibrations. The birefringent medium which is the essential element of such a switch may undergo small dimensional changes due to vibrations, but this will cause little or no effect.

Here, the fractional length change produces no more than an equal fractional change in the phase separation of the two orthogonally polarized components which traverse the medium. In most cases, the phase change will be even less, since length changes are always offset by an oppositely-directed change in refractive index. Such changes, in any case, may degrade the "off" and "on" states of the switch to a slight degree, but this should not represent a predominant feature of system operation.

This study therefore devotes its attention to the effects of vibration in the laser master oscillator. Such vibrations can degrade operation either by (1) varying the cavity length or by (2) bending the mirrors away from a condition of mutual parallelism. Subsequent analysis first considers the effects of bending and then proceeds to the variable length phenomenon.

E.2 NON-PARALLEL END MIRRORS

Consider the case of end-mirrors statically (at first) flexed as in figure E-1. This flexure will support a condition of stimulated emission only if the two right-ward travelling rays have not suffered too large a degree of angular separation. In particular, if the beam diameter is D, and θ_D = far-field divergence angle,

$$D \cdot 2(\alpha - \beta) \leq \lambda/4 \qquad (1)$$

$$\alpha - \beta \leq (1/8)(\lambda/D) = (1/8)\ \theta_D \qquad (2)$$

Thus, the magnitudes of the vibration angles are restricted by the beam diameter. Larger angles will not permit phase reinforce-

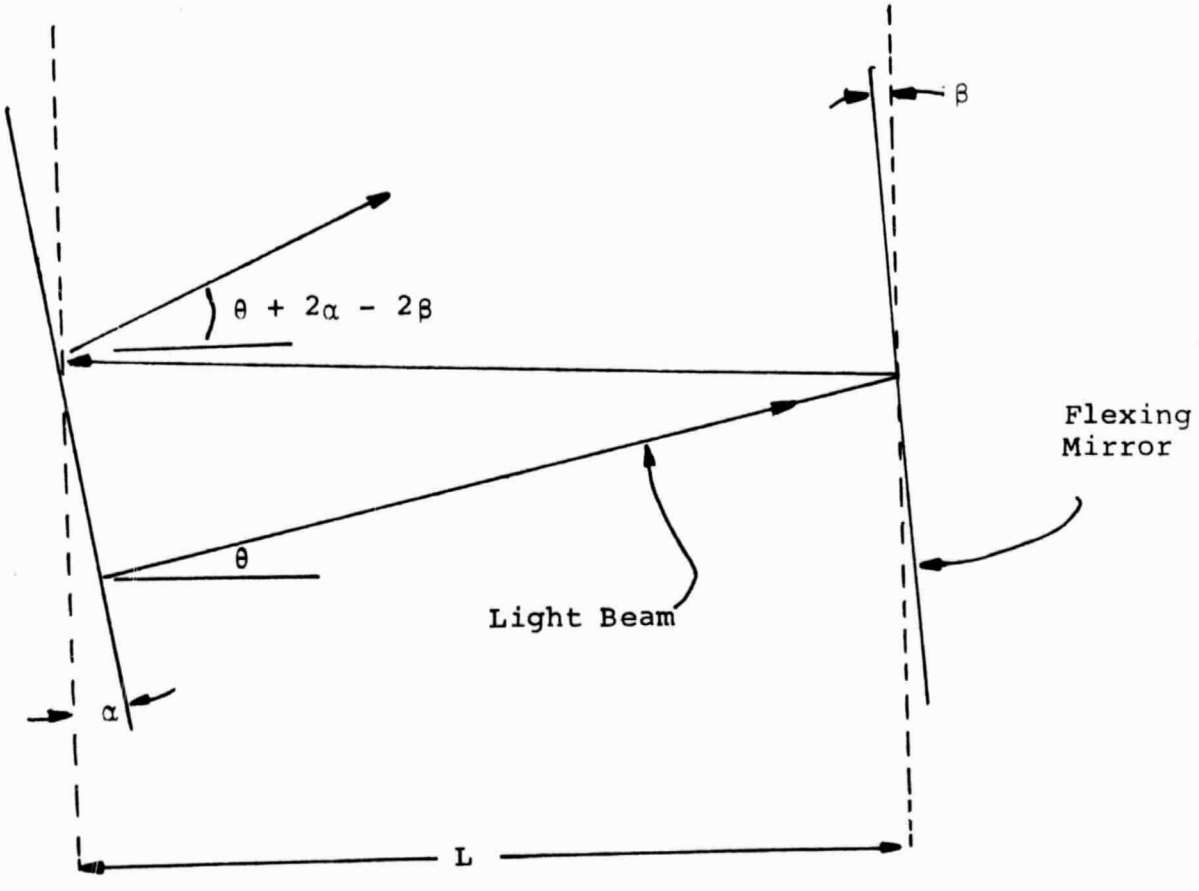

Figure E-1. Graphical Characterization of Mirror Flexure in a Laser Cavity

ment over the entire diameter and power will consequently fall off. The degradation process is not an abrupt one as the above inequalities might at first suggest. It is, rather, a continuing process as confirmed by the following mathematical analysis: The initial wave, as it leaves the left-mirror, conforms to an electric field of

$$\exp i[2\pi\nu t - k(x \sin\theta + z \cos\theta)] \qquad (3)$$

Upon reflecting off the right hand mirror and again off the left one, it re-emerges as

$$\exp i\{2\pi\nu(t + \tau) - k[(x \sin(\theta + 2\alpha - 2\beta) + z \cos(\theta + 2\alpha - 2\beta)]\} \qquad (4)$$

$$\tau = \frac{2\ell}{c}$$

assuming that the intervening lasing medium provides the unity feedback gain characteristic of oscillators. Taking α and β as small, and considering that normal operation corresponds to $\theta = 0$, the re-emerging beam has suffered an effective multiplication of its electric field by

$$\exp i[\omega\tau - 2kx(\alpha - \beta)] \equiv a \qquad (5)$$

Mutual reinforcement of singly, doubly,...,n-tuply,... reflected beams therefore corresponds to a final output given by

$$(\exp i\omega t)(1 + a + a^2 + \ldots + a^n + \ldots) \qquad (6)$$

$$= \frac{\exp i\omega t}{1 - a} = \frac{\exp i\omega t}{1 - \exp i[\omega\tau - 2kx(\alpha - \beta)]}$$

Up to this point, the two mirror positions have been considered as quasi-static, in view of the extremely high speed of the reflecting light wave. Beyond this point, however, α and β may be considered as zero-mean temporal variables, expressing the vibrational flexure of the mirrors.

We may now distinguish between cases in which (i) strong mechanical resonances lead to identifiable sinusoids for α and β, and (ii) where the lack of such resonances reduces them to statistical quantities. For case (i), an equal-magnitudes assumption for α and β leads to

$$\alpha(t) = b \cos \omega_m t$$
$$\beta(t) = b \cos (\omega_m t + \Phi) \qquad (7)$$

ω_m = radian frequency of mechanical resonance

yielding

$$2kx(\alpha - \beta) = -4kxb \sin(\Phi/2) \sin(\omega_m t + \Phi/2) \qquad (8)$$

The exponent in the denominator of (6) characteristically vanishes at resonance indicating that $\omega\tau - 2kx(\alpha - \beta) = 2\pi\eta$, i.e., the optical (radian) frequency ω varies in time as

$$\omega = \omega_o + \frac{4kxb \sin(\Phi/2) \sin(\omega_m t + \Phi/2)}{\tau} \qquad (9)$$

$$\omega_o = \frac{2\pi\eta}{\tau}$$

Since x occupies a continuum of values between $\pm D/2$, the magnitude of the frequency deviation corresponds to substituting

$(x)_{rms} = D/(2\sqrt{3})$ in the above expression. The expected frequency deviation thus varies as

$$\langle \Delta\omega(t) \rangle = \frac{2\pi}{\lambda L\sqrt{3}} bcD \sin(\Phi/2) \sin(\omega_m t + \Phi/2) \qquad (10)$$

According to this relation, the case of $\Phi = 0$ should give $\langle \Delta\omega(t) \rangle = 0$. In apparent contradiction, the physical setup in figure 1 indicates that both mirrors flex in synchronism. It is a condition which clearly tends to shorten the effective linear cavity dimension from L to

$$L \cos \alpha = L \cos(b \cos \omega_m t) \qquad (11)$$

This quantity however deviates from L only as the second power of $b << 1$ and its variability can be neglected, not only for $\Phi = 0$, but for all cases when $\Phi \neq 0$. Case (ii) applies for the absence of any particularly strong resonance. Following a similar line of reasoning as above, it shows that an ideal single frequency output $\omega = \omega_o$ would now broaden into a band of width

$$\Delta\omega = \frac{\pi DC}{L\lambda\sqrt{3}} (\alpha_{rms} + \beta_{rms}) \qquad (12)$$

Since laboratory lasers exhibit a line width of $\delta\omega (\sim 10^4 hz)$, the above phenomenon will effectively increase $\delta\omega$ by $\Delta\omega$ and therefore reduce the power density to a fraction

$$\frac{\delta\omega}{\delta\omega + \Delta\omega}$$

of its original size

E.3 TRANSLATIONAL EFFECTS OF VIBRATION

The remaining vibrational disability concerns relative translation of the two mirrors, lengthening the cavity from its original dimension, L, to L + $\Delta L(t)$. Following previous discussion, laser frequencies correspond to those values of ν which cause

$$1 - \exp[i2\pi f \cdot 2(L + \Delta L)/C] = 0 \qquad (13)$$

Equivalently, the square-bracketed term must reduce to an integer multiple of $i2\pi$:

$$f = \frac{nc}{2(L + \Delta L)} \doteq f_o + f_o \frac{\Delta L(t)}{L} \qquad (14)$$

Again, a strong mechanical resonance will render $\Delta L(t) = d \sin \omega_m t$ resulting in a sinusoidal variation in laser frequency. Noise-like vibrations, on the other hand, tend to enlarge the laser line-width by $f_o (\Delta L)_{rms}/L$ with a corresponding decrease in power density.

E.4 NUMERICAL EXAMPLES

Equation (10) describes the reaction of vibrations on a laser transmitter having a strong mechanical resonance at some frequency $f_m = \omega_m/2\pi$. This case will probably not apply in practice, since any noticeable vibration within a small enough frequency regime to qualify as a mechanical resonance would probably attract sufficient attention from the mechanical designers to invite its (acoustic) suppression. For the sake

of completeness, however, we attempt here to estimate its effect. The ratio $\lambda L/D$, contained in (10), represents the free space spreading of the laser beam within the cavity and will probably not exceed D itself. This is equivalent to setting $D_{max.} = \sqrt{\lambda L}$ and suggests a value of 2mm for the ratio. Inserting this value into (10), we find that the coefficient of the sinusoidal terms reduces to 6×10^{11} b/sec. Quantity b represents the maximum angular deviation of either flexing mirror under the influence of vibrations. In a well-insulated system, this value should not exceed 10^{-3} or 10^{-4} of the diffraction angle $\lambda/D = \sqrt{\lambda/L} = 3 \times 10^{-3}$. Taking the more conservative estimate of 10^{-3} and assuming that $\sin(\phi/2)$ will take on a statistically expected magnitude of 0.7, we see that such vibrations will result in sinusoidal variations in frequency about its expected value. These variations attain a maximum magnitude of about 1 megacycle at a frequency of f_m.

For the non-resonant case, corresponding to (12), similar reasoning shows that the frequency band will broaden by about 10^5hz. Should the unvibrated laser line width achieve a value of 10^4hz, this would correspond to a decrease in power density by a factor of 0.1, although the total power should remain constant.

Finally, fractional changes in cavity length of 10^{-9} will produce results of the same order as above; larger fractional changes will generate proportionately larger frequency excursions or line widths.

E.5 MECHANICAL VIBRATIONS

One reason for susceptibility of an optical laser radar system to mechanical vibrations arises from defects in heterodyne alignment which result from the continuous jolting. In the relatively brief time that it takes a transmitted laser pulse to reflect off a target and return to a coaxial transmitter-receiver system, vibrations may have tilted the antenna. Wavefronts from the optical radar return will then impinge on the antenna in some non-parallel manner with respect to the aperture plane. Since local oscillator radiation is equivalent to a second beam which always enters the antenna aperture in perfectly parallel fashion, the tilting or non-parallelism corresponds to the generation of a fringe pattern. If there are as many light as dark fringes the aperture is essentially averaging over equal strength signals of opposite phases, producing little or no heterodyne output. Less severe tilting reduces the number of fringes to one, or a fraction of one, with a comensurate increase in heterodyne output strength. Problems of this type are particularly important in the airborne laser radar which must attach to a vibrating frame, eg., a CAT detection system.

The present investigation assesses vibration defects in terms of the number of additional pulses needed to produce the same S/N ratio as originally specified for a vibration-free environment. Post-detection pulse integration is assumed. While any general value of integration efficiency may apply, we note here that the widely used case of "square-root" improvement gives a particularly simple result. Square-root improvement indicates an increase in the overall S/N ratio of an n-pulse radar return in proportion to n. It provides a conservative estimate of system degradation, and special attention will therefore be devoted to this case.

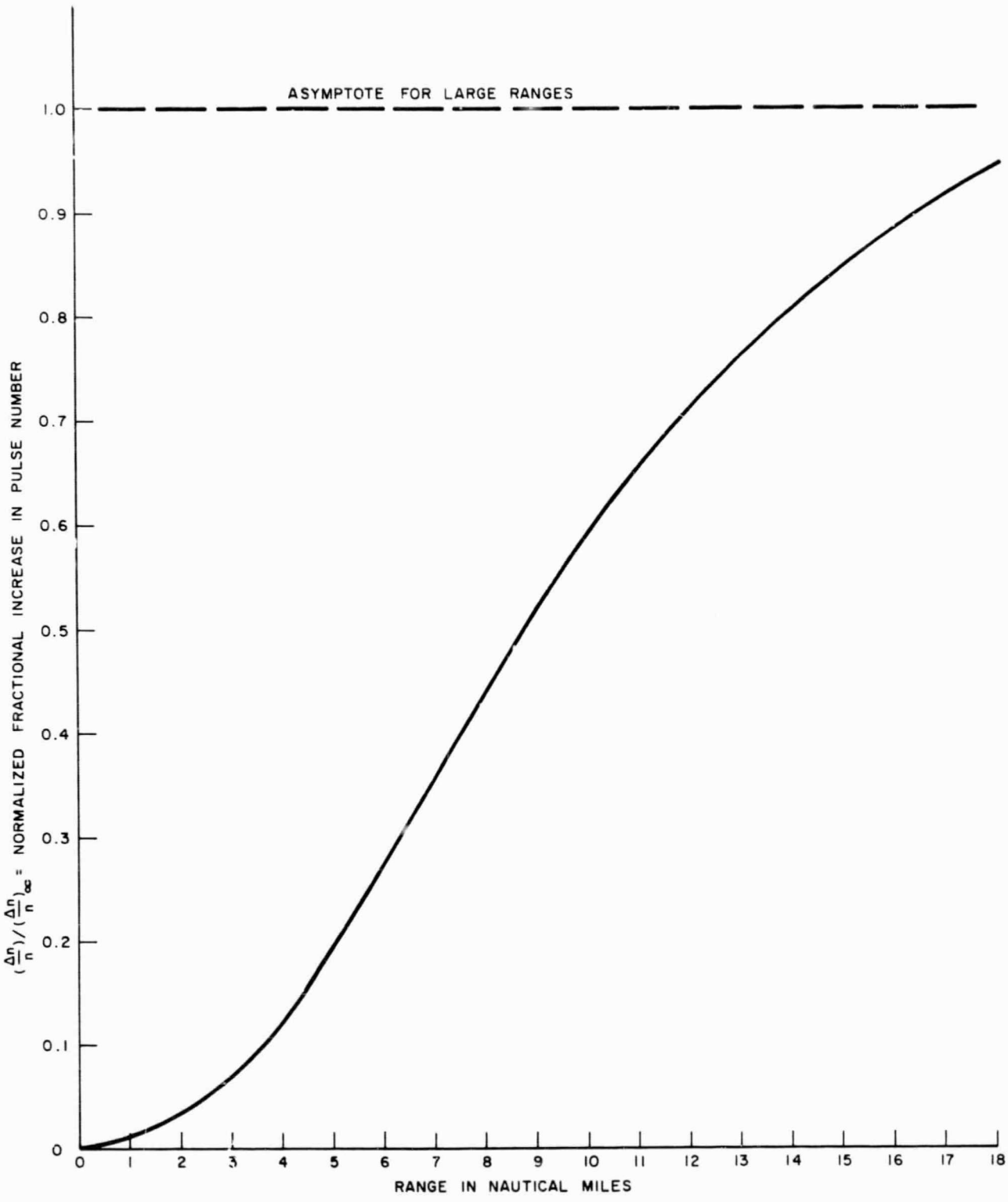

Figure E-2. Variation of Pulse Number with Range

E.6 SUMMARY OF RESULTS

Results may be summarized by means of the graph of figure E-4 or by the equivalent relationship

$$\frac{\Delta n}{n} = 10^{\left(1-\frac{d}{10}\right)} \left(\frac{r}{\lambda}\right)^2 \left(\frac{\delta}{L}\right)^2 \left[1 - \epsilon^{-\left(\frac{4\pi BR}{c}\right)^2/6}\right] \qquad (15)$$

n = number of pulses providing a given S/N ratio in a vibration-free environment.

Δn = number of additional pulses required in a vibrating environment

r = antenna dish radius

λ = optical wavelength

δ = representative vibrational displacement of surrounding environment

L = mounting base dimension

B = vibration noise bandwidth

R = radar range

c = velocity of light

d = decibels attenuation of vibration provided by shock mounts

This expression may be rewritten as

$$\left(\frac{\Delta n}{n}\right) \Big/ \left(\frac{\Delta n}{n}\right)_\infty = 1 - \epsilon^{-.0096\ (B/\ kc.)^2\ (R/\ n.mi.)^2} \qquad (16)$$

where $\left(\frac{\Delta n}{n}\right)_\infty$ represents the limiting value of $\left(\frac{\Delta n}{n}\right)$ when either the range or the noise bandwidth has become arbitrarily large. Either limiting process, it will be noted, corresponds to the physical limitation of absolutely no correlation (from one radar pulse to the next) in successive antenna orientations when subjected to a vibrating environment.

Equation (16) may be expressed graphically, as in the curve of Figure E-2. A vibration bandwidth of one kilohertz is assumed,

since this number is representative of bandwidths encountered in many aircraft. Similar information for other bandwidths of, say, k kilohertz can also be obtained from this curve provided that an indicated range of M nautical miles is interpreted as an actual, physical, range M/k nautical miles.

Normalizing factor

$$\left(\frac{\Delta n}{n}\right)_{\infty} = 10^{\left(1-\frac{d}{10}\right)\left(\frac{r}{\lambda}\right)^2 \left(\frac{\delta}{L}\right)^2} \qquad (17)$$

shows that the additional number of pulses required increases as the square of the antenna size, as measured in optical wavelengths; a rather critical quantity. By the same token, an increase in mounting base dimensions, typified by L, will tend to reduce the required additional pulses in an inverse square law manner. This, of course, assumes sufficient rigidity for the base, so that the same representative vibrations applied to a longer (rigid) moment arm result in smaller angular deviations. Attenuation constant d generally assumes values of about 30 db or greater for currently available shock mounts. At lowered vibrational frequencies, which might promote a mechanical resonance condition for the shock-mounted unit, d will tend to decrease in size and will sometimes turn positive. Such an amplification condition results from a too-small mass for the laser radar unit, resulting in an underdamped situation. This, of course, can be corrected through additional weight and/or damping.

Quantity n, it should be remembered, is still a function of range R. Thus, the ratio of $\frac{\Delta n}{n}$ to $\left(\frac{\Delta n}{n}\right)_{\infty}$ may vary with R in a manner given by the right side of (16) but Δn will vary with R in a manner which is proportional to the right side of (16) and to n(R) as well. (For square-root law post detection integration, it can easily be shown that n(R) varies as R^2.)

E.7 NUMERICAL EXAMPLES

As an example of these calculations, we take

δ = 0.1 millimeter

L = 1 meter

r = 12 inches

λ = 10 microns (CO_2 laser)

d = 34 db.*

B = 1 kc

R = 1 n mi, 10 n mi respectively

Then, for the 1 n.mi. case, the curve of figure E-1 and/or equation (16) shows that

$$\left(\frac{\Delta n}{n}\right) = .0096 \left(\frac{\Delta n}{n}\right)_\infty$$

Equation (3) meanwhile gives

$$\left(\frac{\Delta n}{n}\right)_\infty = 10^{-2.4} (3 \times 10^4)^2 (10^{-4})^2 = .036$$

Thus, if n = 100 pulses, $\Delta n = (.0096)(.036)(100) \sim .036$ i.e., no additional pulses needed.

For the case of 10 n.mi.

$$\left(\frac{\Delta n}{n}\right) = .6 \left(\frac{\Delta n}{n}\right)_\infty = .6\ (.036)$$

since $(\Delta n/n)_\infty$ remains the same. The same requirement of n = 100 pulses now gives Δn = 2.16 pulses i.e., 2 pulses. Even at large ranges, no more than 4 additional pulses would ever be required. Note, however, that the situation becomes more critical if δ = 1 millimeter and d = 24 db. All foregoing values of Δn would increase by 100:

R = 1 n.mi	Δn = 3.6
R = 10 n.mi	Δn = 216
R = ∞	Δn = 360

* This figure obtained from "Isolation Efficiency Curve for Flexible Mounting Systems", presented in the Lord Manufacturing Company General Catalog LB-1300

E.8 ANALYTIC APPROACH

Proof of these results follows from calculating (i) the effective degradation due to a static tilt in the antenna, (ii) the statistically expected value of this degradation when angular tilting varies randomly with time, (iii) the additional pulses required to compensate the degradation via post-detection. Static tilting degradation can be characterized by a $[J_1(x)]/x$ -type fall-off from unity (or 100% efficiency) where x essentially represents the angle of tilt, and J_1 refers to the first order Bessel function. This curve, like the closely related (sin x)/x, can be approximated by e^{-kx^2} for appropriate values of k - a decided convenience in computing statistical expectation, under (ii). For square-root law integration improvement, the number of additional required pulses follow from the relatively simple relations in (i) and (ii). For the more general α -law improvement ($1 \geq \alpha \geq .5$; $\alpha=1$ signifies pre=detection integration), analytic results still follow directly, but are most conveniently expressed in terms of the total number of pulses, $n + \Delta n$, rather than Δn alone.

E.9 EFFECTIVE ANTENNA DEGRADATION

Given a circular aperture antenna tilted by an angle θ with respect to an incoming radar return, as in figure E-3

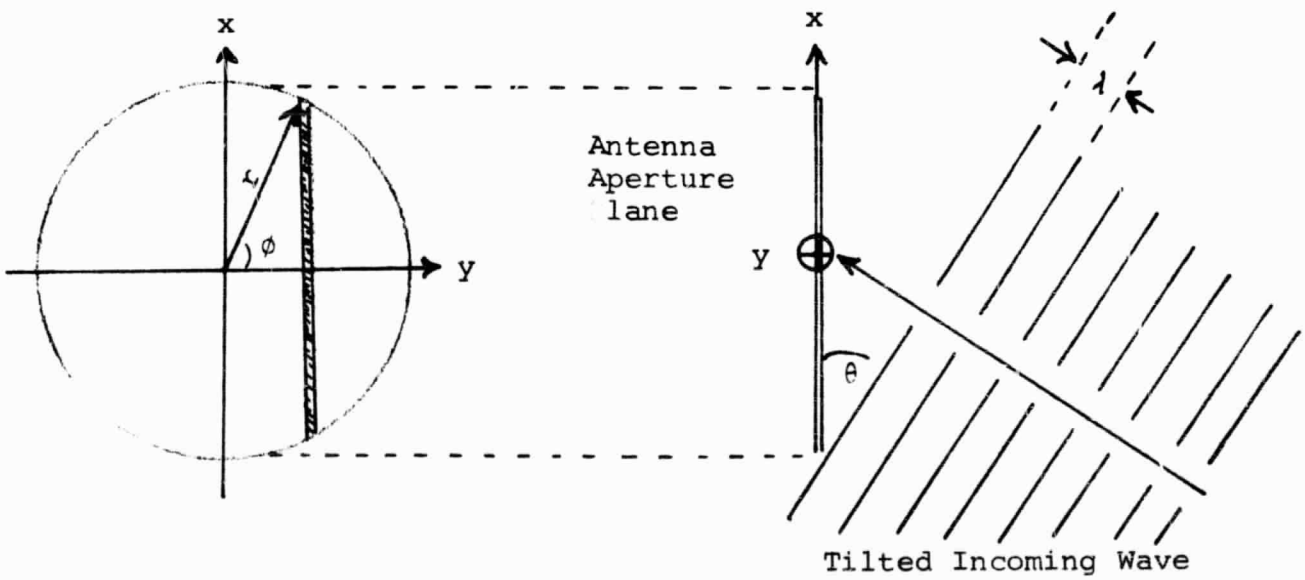

Figure E-3. Physical Aspects of Antenna Degradation

the electric field impressed on the typical (shaded) vertical slice will vary as exp [i $(2\pi/\lambda)$ x sinθ]. Since the local oscillator radiation is equivalent to a second incoming wave characterized by $\theta = 0$, the foregoing exponential term is also proportional to the signal-carrying portion of the received optical intensity and, therefore, to the differential contribution to the photocurrent from the element of the shaded slice between x and x + dx. Integrating over the entire shaded slice, the photocurrent contribution will vary in proportion to

$$(\lambda/\pi \sin\theta) \sin [(2\pi r \sin\theta \sin\phi)/\lambda] \cdot d(r\cos\phi)$$

The total photocurrent therefore follows from integrating this quantity from $\phi = -\pi$ to $\phi = 0$, equivalent to integrating over all slices from y = -r to y = +r, and yields a result proportional to

$$\pi r^2 \cdot \frac{2 J_1 (2\pi \frac{r}{\lambda} \sin\theta)}{2\pi \frac{r}{\lambda} \sin\theta}$$

$$\doteq \pi r^2 \cdot \exp [-\sin^2\theta/2 (\lambda/\pi r)^2] \qquad (18)$$

The exact expression, in terms of J_1, appears graphically in figure E-4. It shows that smaller antenna dishes may receive less signal than larger ones, but do not react as sensitively to tilting.

E.10 STATISTICALLY EXPECTED VALUE OF ANTENNA DEGRADATION

Based on the approximation in (18), we seek to find the expected value of $f(\theta) = \exp [-\sin^2\theta/2(\lambda/\pi r)^2] \doteq \exp [-\theta/2(\lambda/\pi r)^2]$ given the Gaussian probability distribution $(1/\sigma\sqrt{2\pi}) \exp (-\theta^2/2\overline{\theta^2})$, where $\overline{\theta^2}$ = mean square value of angular tilting in a given dynamic situation. Since f (θ) and the probability distributions are both Gaussian, the result follows quite easily as

$$\langle f(\theta) \rangle_{\text{expected}} = \sqrt{\frac{(\lambda/\pi r)^2}{\overline{\theta^2} + (\lambda/\pi r)^2}} \qquad (19)$$

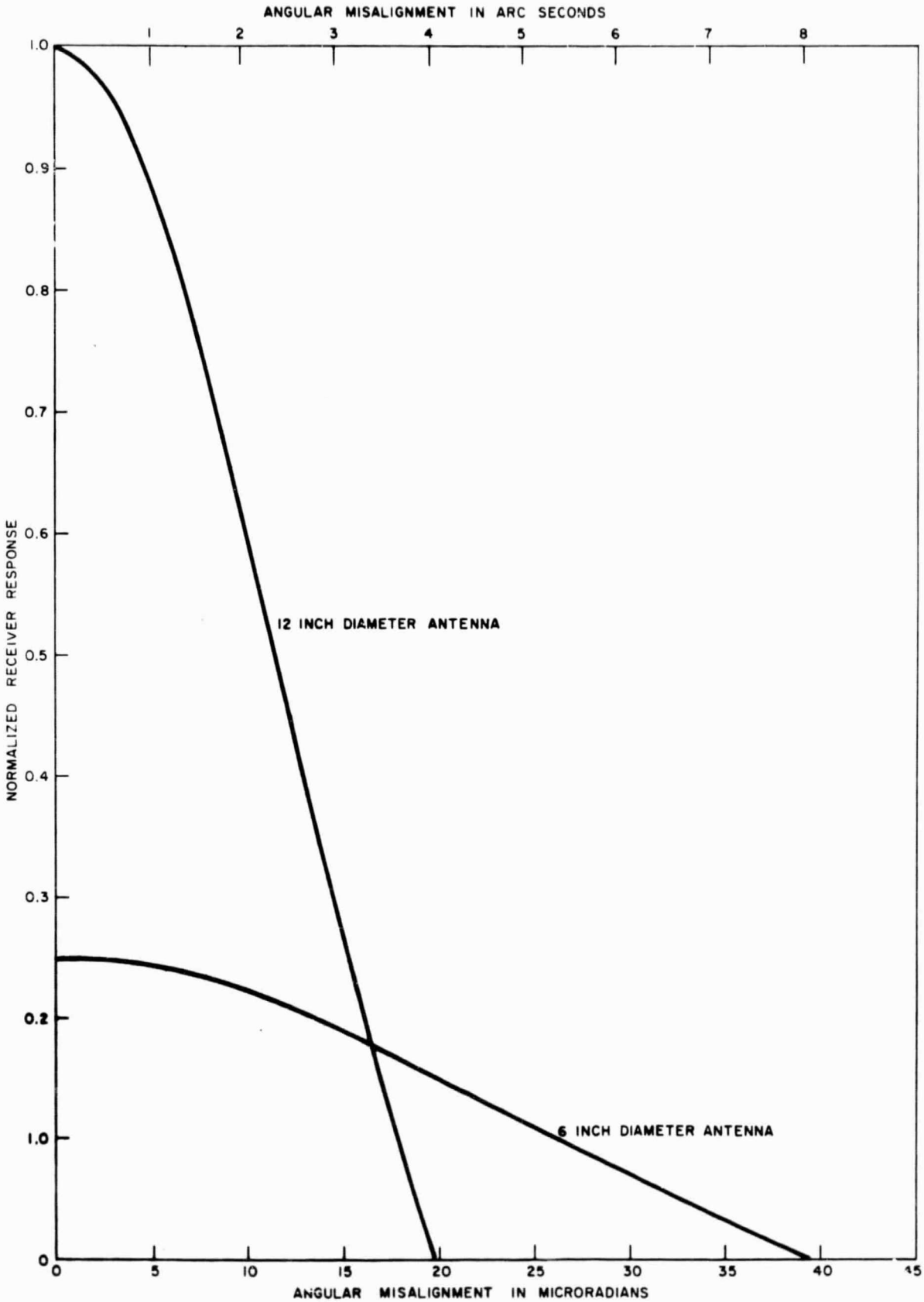

Figure E-4. Antenna Degradation Due to Static Tilt

Degradation clearly becomes worse as $\overline{\theta^2}$ and/or (r/λ) increase. These results, because of the assumption of the above Gaussian, assume no pulse-to-pulse correlation in successive antenna positions. Correlation will be explored separately, in a later section of this analysis.

E.11 PULSE INTEGRATION IMPROVEMENT

To compensate the degradation of $\langle f \rangle$ from an optimum value of unity, the number of pulses may be increased. When no vibration occurs,

$$(S/N)_n = (S/N)_1 \, n^{\gamma}$$

where $(S/N)_1$ = per-pulse S/N ratio, $(S/N)_n$ = increased S/N ratio resulting from post-detection integration, of n pulses and γ = a function of n and probability of false alarm, ranges between 0.5 and 1. Due to vibration, (S/N), which varies in proportion to received power, and thus, in proportion to <f>, changes to $(S/N)_1$ <f>. To maintain the same $(S/N)_n$, the pulse number must increase from n to $n + \Delta n$ in a manner given by

$$(n + \Delta n)^{\gamma} \langle f \rangle = n^{\gamma} \qquad (20)$$

or that

$$\frac{n + \Delta n}{n} = \left(1 + \frac{\overline{\theta^2} \, \pi^2 \, r^2}{\lambda^2} \right)^{(1/2\gamma)} \qquad (21)$$

For $\gamma = .5$ this relation reduces to

$$\frac{\Delta n}{n} = \pi^2 \left(\frac{r}{\lambda} \right)^2 \overline{\theta^2} = \pi^2 \left(\frac{r}{\lambda} \right)^2 \overline{\left[\phi \cdot .10^{-\left(\frac{d}{20} \right)} \right]^2} \qquad (22)$$

where ϕ refers to angular tilting in the vibrating environment, θ represents the dimished angular tilting of the antenna, and d gives the decibels attenuation required from shock mounts, to reduce one to the other. Setting $\phi = \delta/L$ now recasts (22) in the form given in (17): a subscript of ∞ indicates that pulse-to-pulse correlation has not yet been assumed.

E.12 MITIGATING EFFECTS OF PULSE-TO-PULSE CORRELATION

The preceeding analysis provides worst-case estimates by virtue of using $\overline{\phi^2}$ = mean square deviation in ϕ from its nominal non-vibrating position. In a practical situation, however, a radar pulse may be emitted and received for vibration angular deviations of $\phi(t)$ and $\phi(t + \tau) \equiv \phi[t + (2R/C)]$ respectively. Under these conditions, $\overline{\phi^2}$ should be replaced by

$$\overline{\tfrac{1}{2}[\phi(t+\tau) - \phi(t)]^2} = [\overline{\phi^2} - \overline{\phi(t+\tau)}] = \overline{\phi^2}[1 - \rho(\tau)] \qquad (23)$$

An approximate form for $\rho(\tau)$ follows from the Wiener Khinchine theorem: where $\rho(\tau)$ = normalized autocorrelation function of $\phi(t)$. If $\phi(t)$ corresponds to a bandwidth of B, its noise power spectrum may be represented by

$$|\Phi(f)|^2 = |\Phi(0)|^2 \text{ rect } \frac{f}{2B} \qquad (24)$$

where rect x = 1 for $|x| < 1$, but otherwise vanishes. According to the Weiner theorem the inverse Fourier transform of $|\Phi(f)|^2$ gives the autocorrelation function:

$$\rho = \frac{\sin 2\pi B\tau}{2\pi B\tau} = \frac{\sin (4\pi BR/c)}{4\pi BR/c} \doteq \epsilon^{-(4\pi BR/c)^2/6} \qquad (25)$$

We therefore rewrite (22) as

$$\frac{\Delta n}{n} \pm 10 \frac{r}{\lambda} \overline{\phi^2}\,[1 - \rho(\tau)]\; 10^{-\left(\frac{d}{10}\right)} \qquad (26)$$

taking $\pi^2 \doteq 10$. Inserting the expression for ρ as given in (25), and replacing $\overline{\phi^2} = \overline{(\delta/L)^2}$, equation (26) reduces finally to the original expression in (1). Note that as $B \to \infty$ or $R \to \infty$, $\rho(\tau) \to 0$ and $(\Delta n/n) \to (\Delta n/n)_\infty$.

E.13 CONCLUSION

The preceding study of a vibrational environment on a laser radar system points to the need for keeping vibrational

displacements less than 1mm, shock mount isolations greater than about 30db and vibration noise bandwidths (as seen by the radar system) less than 1kc. There is no particular advantage however, to decreasing the antenna size: Equation (1) shows that Δn varies in proportion to r^2, i.e., to the antenna aperture area. Suppose a new receiving antenna of area 1/M of the original.* This will tend to reduce Δn by a factor of M. But, the received power and S/N ratio will both decrease by a factor of M, requiring $M^{1/\gamma}$ times as many pulses to compensate the defect. This tends to increase Δn by a factor of $M^{1/\gamma}$, so that the net change in Δn corresponds to a factor of $M^{(1/\gamma - 1)} > 1$ i.e., an increase.

If, however, the decrease in receiving antenna area is compensated by operating M such receivers in parallel, the signal strength will increase by $\sqrt{M}$, and the requirement on Δn will relax by a proportionate amount, i.e., Δn now changes by a factor of $M^{(1/\gamma - \frac{3}{2})}$, so that any $\alpha > .67$ will permit this technique to reduce vibration susceptibility. This expedient would not of course be attempted until all opportunities to attenuate the vibration amplitude and narrow the noise bandwidth had been exhausted.